

Contact Distribution Encodes Frictional Strength

Sam Dillavou^{1,2}, Yohai Bar Sinai^{1,3,4}, Michael P Brenner^{1,5}, Shmuel M Rubinstein^{1,6}

¹*John A Paulson School of Engineering and Applied Sciences,
Harvard University, Cambridge, MA 02138, USA*

²*Department of Physics, Harvard University,
Cambridge, MA 02138, USA*

³*The Raymond and Beverly Sackler School of Physics and Astronomy,
Tel Aviv University, Tel Aviv 69978, Israel*

⁴*Google Research, Tel Aviv, Israel*

⁵*Google Research, Mountainview CA, USA*

⁶*The Racah Institute of Physics,
The Hebrew University of Jerusalem,
Jerusalem, 91904, Israel*

(Dated: May 4, 2022)

The static friction coefficient, μ , is a central quantity in modeling mechanical phenomena. However, experiments show that it is highly variable, even for a single interface under carefully controlled experimental conditions. Traditionally, this inconsistency is attributed to fluctuations in the real area of contact between samples, A_R . In this work, we perform a variety of experimental protocols on three pairs of solid blocks while imaging the contact interface and measuring μ . Using linear regression and images of the interface taken prior to tangential loading, we predict the static friction coefficient. Our model strongly outperforms two benchmarks, the Bowden and Tabor picture ($\mu \propto A_R$) and prediction using experimental variables, indicating that a large portion of the observed variance in the initialization of slip is encoded in the contact plane. We perform the same analysis using only sub-sections of the interface, and find that regions as small as 1% of the interface can still beat both benchmarks. However, bigger sub-sections of the interface, even when comprised of many small regions with bad individual predictive power, outperform the best small regions alone, suggesting that the interfacial state is not dependent on any single point, but is rather distributed across the contact ensemble.

Static friction, the force required to initiate sliding between two solid bodies, is a highly variable quantity. Not only does it depend on a large variety of known factors, both controlled [1–10] and uncontrolled (such as wear) [9, 10], but it can also vary significantly and unpredictably between successive identical experiments using the same two bodies [9]. This stochasticity largely stems from one inconvenient truth about frictional interfaces; even using the same bulk solids, a new system is formed after each slide. Each such interfacial system contains the ensemble of contact points between two rough bodies, which typically cover a small fraction of the interface due to surface roughness. The frictional strength is classically considered a linear function of the total real contact area of an interface A_R , as the two quantities generally evolve in tandem [1, 5, 11–15]. However, in recent years it has been shown that this is not always the case; an interface may strengthen while its real area of contact shrinks [10], or vice versa [16]. These deviations from the classical picture have several known physical sources, such as the evolution of interfacial bonding [2], the heterogeneous nature of contact evolution [10, 17], the role of interfacial geometry [9, 17, 18], and dynamics of slip nucleation. Once larger than a critical length scale L_C , a slipping region of the interface will propagate much like a classical fracture [19, 20]. However, below this scale little is known about mechanics of slip nucleation, as they are notoriously difficult to measure.

The state-of-the-art predictive model, known as Rate and State [21–23], ignores much of this complexity, as it is a phenomenological model with typically only one (but at most a handful of) degree(s) of freedom. As a result, it is a reasonable but crude approximation of static frictional strength and a subject of continual debate [24]. While it is known that the interfacial state is more complex than Rate and State can describe [8–10], the true degree of complexity required to predict frictional strength, and what is necessary to measure, is still an open question.

Predicting a single number, such as μ , from a complex data set is a canonical data science problem. Exciting progress has been made predicting laboratory or real earthquakes by utilizing flexible and complex methods like convolutional neural nets or boosted decision trees, [25–28]. In closely related works, similar methods were used to predict mechanical failure of rocks [29] and amorphous solids [30]. However, these methods create an additional layer of complexity, further obfuscating the physical processes themselves. As a result, any successful prediction is extremely difficult to interpret. Furthermore, the majority of these works utilize signals that are readily measurable for real earthquakes, e.g. acoustic emissions, but do not provide direct measurement of the internal interfacial state. Some prediction work has been done using direct measurements from bi-material model faults [28], but with equally complex algorithms, and it is unclear if these results apply to single material, multi-

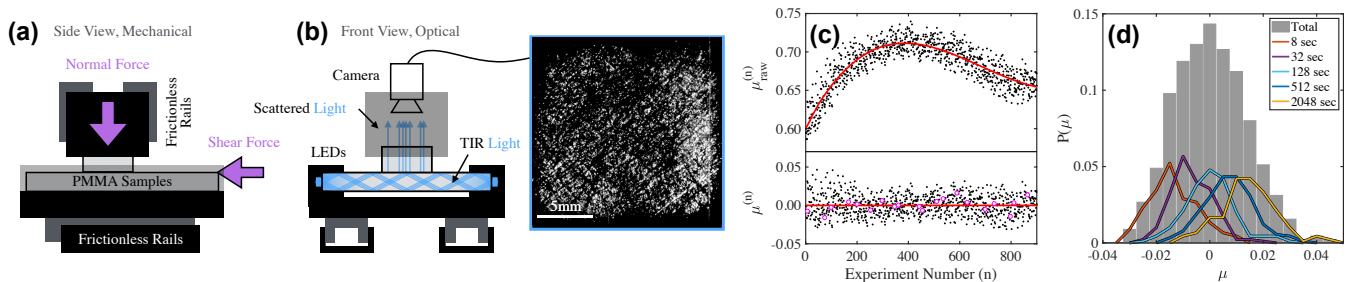


FIG. 1. Experimental Setup a) Schematic of the biaxial compression/translation stage. b) Embedded optical setup and example image of interfacial contact for block pair 1 at experiment number 100. c) $\mu_{raw}^{(n)}$ and $\mu^{(n)}$, versus experiment number n for block pair 1. Raw data is de-trended using a 3rd order polynomial fit shown in red. Data with $t=128s$, $S=20N$ is highlighted in magenta. d) Histogram of the static friction values from (c). Color histograms highlight time dependence.

contact interfaces. Together, these methods indicate that friction is indeed predictable, but give no list of ingredients or recipe. Furthering our physical understanding therefore requires predicting frictional strength from direct measurements of the interface in a straightforward and comprehensible manner.

Here we use linear regression to predict the static friction coefficient of a multi-contact interface smaller than L_C , using images of its static real area of contact and no other inputs. This method is 50% more accurate than two benchmark methods using total area of contact and experimental parameters, indicating that a significant portion of the unexplained variance in frictional strength is encoded in the real area of contact. Due to the linear nature of our regression, we may perform the same analysis using arbitrary portions of the interface. We find some regions as small as 1% of the interface still outperform the two benchmarks. However, large fractions of the interface, even if they are composed of regions that were poorly predictive on their own, outperform the best small regions, suggesting that state of an interface smaller than L_C is dependent on the entire contact ensemble.

Experiments are performed separately on three pairs of laser-cut PMMA (poly methyl-methacrylate) blocks with 1 - 2.5 cm² of nominal contact area. The bottom samples are original, extruded PMMA (11nm RMS), approximately 60x100x4mm, which are directly contacted by the horizontal force sensor. The top samples are lapped with 1000 grit polishing paper (~ 800 nm RMS), and are the main source of variance between interfacial systems. All samples are washed with soap, then rinsed with deionized water, then isopropanol, and finally air dried. The biaxial compression and translation stage used to measure the friction coefficient is described in detail in a previous work [10], and shown schematically in Fig 1(a). Single-wavelength (473nm) light is injected into the bottom sample where it remains trapped through total internal reflection, except at points of actual contact with the top sample. As a result, when imaged from above, the brightness of the interface corresponds to points of real

contact, as shown for a typical example in Fig 1(b). The position camera is fixed in relation to the top (smaller) block. Images are subsequently reduced in pixel count by a factor of 4, 16, or 100 (for κ_2 , κ_3 , and κ_1 respectively, see Eq. (2)) by square-kernel max pooling. This reduction speeds computation and reduces over fitting.

All experiments are conducted using the standard Slide-Hold-Slide (SHS) protocol. Under constant normal load, $F_N = 90N$, samples are slid at 0.33 m/s to reset the interface. The interface is then held static for time t sec under constant shear load S N. The set of S and t combinations used for each block pair is distinct, with 45, 54, and 25 unique combinations for pairs 1, 2, and 3 respectively. For details see [31]. At this point, an image of the contact plane is taken and subsequently the sample is loaded at a rate of 0.33 mm/s until the initiation of slip, accompanied by a sharp drop in the measured shear force. We define μ_{raw} as the highest shear force prior to slip, or the ‘static peak’, divided by the normal load. To avoid systematic biases, the experiments are ordered such that every possible combination of experimental variables is performed once in a random order, then again in a different random order and so on.

μ_{raw} varies significantly between subsequent measurements, but also displays a slow, non-monotonic drift over many hundreds of experiments, as shown in Fig 1(c), top. This second effect is due to wear of the surfaces, and is interesting in its own right. Here, however, it obscures the variance between proximal measurements. Subtracting a 3rd order polynomial fit of the data from μ_{raw} isolates the rapid fluctuations we wish to study, as shown in Fig 1(c), bottom. Because it is not possible to de-trend images of interfacial contact, this process renders prediction more difficult but also more focused; any prediction must ignore the interfacial changes that result in this slow drift while simultaneously picking up on those that create the experiment-to-experiment fluctuations. For this reason the de-trended data, μ , will be used for the remainder of this letter. As expected, μ has a systematic but noisy dependence on the experimental variables such as time t ,

as shown in Fig 1(d), which will be used as a benchmark.

Like most physical (non-digital) systems, our data collection is limited by real-world constraints [32]. Block pairs can be used for only a few hundred to one thousand experiments before they are worn beyond use. As a result the problem is massively under-constrained, and we must limit the complexity of our model. Predictions of μ are made by linearly weighting the (grayscale) pixels of the corresponding image $\{p_{ij}\}$. Explicitly, the prediction for n -th friction measurement, $\hat{\mu}^{(n)}$ is

$$\hat{\mu}^{(n)} = C + \sum_{ij} p_{ij}^{(n)} w_{ij} \quad (1)$$

where C and w_{ij} are fitting parameters (“weights”) that are constant for the entire data set, and are found by minimizing the squared error of the predictions. We add a regularization function κ to this error to discourage over-fitting. That is, we solve for C and w_{ij} by minimizing the loss function

$$w_{ij}, C = \arg \min \left\{ \sum_n (\mu^{(n)} - \hat{\mu}^{(n)})^2 + \alpha \kappa(w_{ij}) \right\} \quad (2)$$

where α is a hyper-parameter, found for each method by minimizing the cross-validation error within the training set for block pair 1 only. α values are then blindly transferred to block pairs 2 and 3. $\kappa(w_{ij})$ is one of three regularization functions:

$$\kappa_1 = \sum_{ij} (\nabla w)_{ij}^2 \quad \kappa_2 = \sum_{ij} w_{ij}^2 \quad \kappa_3 = \sum_{ij} |w_{ij}| \quad (3)$$

These functions reduce over-fitting by penalizing three different aspects of w_{ij} . κ_1 penalizes spatial gradients, promoting smoothly varying weights. κ_2 and κ_3 produce the standard Ridge and Lasso regressions, respectively. The former promotes smaller weights and is a standard choice of a regularizer when no better prior is known, while the latter promotes sparseness of w_{ij} [33]. Using each of the three κ functions, Eq. (2) is solved with a randomly selected 82% of our data (the training set). The three regularization functions result in distinctly different solutions for w_{ij} , as shown for typical values in Fig. 2.

The accuracy of these regression methods is tested using Eq. (1) with the calculated w_{ij} and C values to predict the remaining 18% of the data that was not used for training (the validation set). We define the prediction error E as the mean of the square of the difference between $\hat{\mu}$ and μ only for the validation set:

$$E = \text{mean} \left\{ (\mu^{(n)} - \hat{\mu}^{(n)})^2 \right\} \text{ (validation set only)} \quad (4)$$

We repeat this process 5 times, each with a unique, randomly chosen set of data points withheld for validation.

All three regularization functions ($\kappa_1, \kappa_2, \kappa_3$) perform strikingly well when their prediction error E_κ is compared

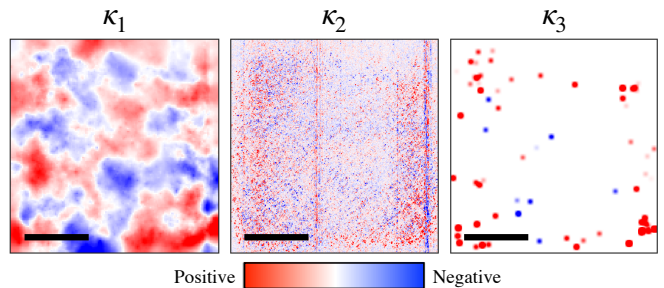


FIG. 2. Visualization of typical values of w_{ij} for three regularization methods using block pair 1. Scale bars are 5mm.

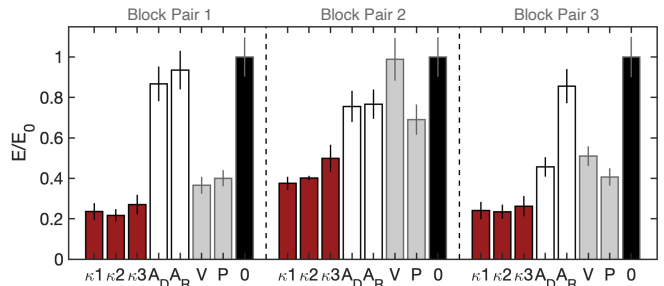


FIG. 3. The interface encodes frictional strength. a) Mean prediction error E normalized by the error when predicting $\hat{\mu} = 0$ for three blocks pairs. Three linear regression methods (κ_i) shown in red are compared with four methods using global variables: the parameter (P) and vicinity (V) methods shown in gray, and the total area of contact, raw (A_R) and detrended (A_D) shown in white. $\hat{\mu} = 0$ (0) is shown in black as a benchmark. Error bars indicate standard deviation across five randomly chosen validation sets for the linear regression methods, and 200 randomly chosen validations sets for the other methods.

to several traditional means of prediction, as shown in Fig 3. Calculating $\hat{\mu}$ as a linear function of the total real area of contact,

$$\hat{\mu}(A_R) = \mu_0 + \sigma A_R \quad A_R = \sum_{ij} p_{ij} \quad (5)$$

gives an error E_A at best 50% higher than our data-driven approach, as shown in Fig 3. Note that converting from A_R to μ requires an offset (μ_0) due to de-trending from μ_{raw} .

It is worth emphasizing that our regression model is quite distinct from the classical method of aggregating contact area; with only a single normal load, we find variations in total A_R to be virtually uncorrelated with variations in μ . Like μ_{raw} , A_R drifts slowly due to wear. Thus, to provide the fairest test, A_R is detrended in the same manner as μ (by subtracting a 3rd order polynomial fit) to produce A_D . A_D does provide slightly better predictions than A_R , as shown in Fig 3, but at best still produces an error 50% higher than our regression methods, which utilize the *distribution* of contact, not just its

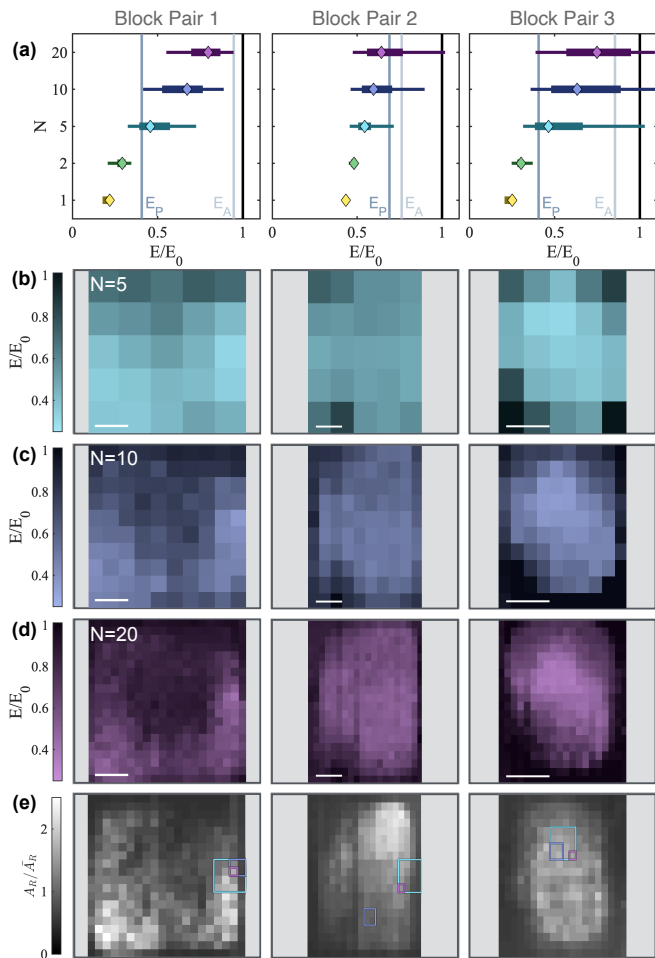


FIG. 4. Prediction error from interfacial subsections for three samples (columns). a) Normalized error E/E_0 for individual interfacial subsections of varying sizes ($N = 1, 2, 5, 10, 20$). Median (diamond), quartiles (thick line), and 5/95 percentiles (thin line) are shown for each size. Data includes five random training/test splits for each region. Benchmark errors for predictions using contact area (light gray), and the parameter method (dark gray) are overlaid for comparison. b-d) Interfacial heat maps of E/E_0 for $N = [5, 10, 20]$. Scale bars are 3mm. c) Average real area of contact across all experiments, down-sampled to 20 by 20. Superimposed frames represent the highest-accuracy regions from (b-d).

sum total. That is to say, the static contact distribution has a strong and non-stochastic connection to fluctuations in frictional strength in an extended multi-contact interface.

Calculating $\hat{\mu}$ using experimental parameters, that is, predicting the mean value of all training set data with the same protocol,

$$\hat{\mu}(S, t) = \text{mean} \left\{ \mu^{(n)}(S, t) \right\} (\text{training set}) \quad (6)$$

is more effective than using A_R or A_D , but at best gives an error E_P that is 50% higher than all E_κ . This is referred to as the *parameter* method. Finally, a prediction

is made using the mean of the previous and the next experiment with the same S and t , which we refer to as the *vicinity* method [34]. This method represents the additional information gained by proximity in time. Interestingly, this method slightly outperforms the parameter method for block pair 1, while under-performing for the other two blocks pairs, suggesting that experiments do not always correlate in time beyond the general (removed) trend. Regardless, for all systems the results fail to reach the accuracy of our regression methods.

The success of the regression model indicates a connection between the geometrical distribution of contact and frictional strength, however it is important to consider how the model makes that connection. It is likely that the model is in part learning two known facets of the interfacial state, the time t and shear S values of each experiment. This is well within its ability; an identical linear regression model trained to predict these values from interfacial images can do so with 95% accuracy. However, because the regression model consistently outperforms the parameter method, the model must be using other (unknown) facets of the underlying state of the interface in addition to S and t . With such a transparent, simple model, it is tempting to directly use w_{ij} to interpret these aspects of the interfacial state. Unfortunately, the solutions are still over-fit; training error reduces to a small fraction of validation error for each regression method. Thus, while the regression *is* learning aspects of this interfacial system that apply beyond its training set, it is also assigning weight to quirks of specific experiments that only pertain to training data. It is therefore difficult to directly assign meaning to w_{ij} values, but also means we may explore further restricting the degrees of freedom in our model.

One means of restriction is dividing the interface into an N by N grid and predicting $\hat{\mu}$ using each sub-section alone. This subdivision allows us to probe the global information gleaned from contact fluctuations in a particular location. For each $(1/N^2)$ th of the interface, our regression analysis is performed using κ_2 , which generally performed best, for regularization and completely ignoring the other regions of the image. The same hyper-parameter α_N is used for all subsections of the same size, again determined by minimizing cross validation on block pair 1 only. Larger areas (smaller N) are better predictors of frictional strength, as shown in Fig 4(a). Typically, areas with higher contact area are also better predictors, as shown by comparing Fig 4(b-d) with 4(e).

Interestingly, some small regions are excellent predictors of μ . For each sample pair there is at least one region with $N = 10$ (1% of the interface) that generates a lower error than all benchmarks. For each sample pair, the most predictive regions for $N = 5, 10$, and 20 cluster in one location, nearly always overlapping, as shown in Fig 4(e). This clustering is especially clear in block pairs 1 and 3, where predictive strength varies strongly across

the interface. Importantly however, these small regions are never as predictive as the average $N = 2$ region, ruling out the possibility that fluctuations in one location alone dictate μ . In fact, with the exception of regions with no contact, our regression method always provides better predictions when given more of the surface as an input. That is to say, information is not only encoded in one locale, but rather the entire ensemble.

We have shown that the distribution of interfacial contact encodes information about frictional strength. Using a simple linear model, even some small subsections of the interface are capable of producing better predictions than the experimental parameters. Without further experimental exploration, such as capturing the dynamics of rupture, we cannot know for sure what physical mechanism gives these regions their superior predictive ability. It is possible that these are regions that contains weak contact or high residual stress likely to nucleate slip, or regions that contain ‘barriers,’ strong contact regions that stop fledgling slips from propagating to the entire system [35]. The excellent predictions are not however an indication that all other points are irrelevant; using the entire interface is always substantially more accurate than using any small region. Furthermore, increasing the size of a region always decreases its prediction error, indicating that the global strength is a function of the entire contact area; while some regions may be more important, they do not contain sufficient information to ignore the rest of the interface.

The as-yet unsolved mechanics of nucleation are not contained within our linear regression model, and our solutions w_{ij} are not transferable or general, as they are based on the specific details of a data set from a single pair of blocks. However, our model has shown that correlating features of a map of contact points to frictional strength is feasible and out-performs traditional predictions. Generalizing this approach to include more complex features and multiple interfacial systems is a promising avenue for future work.

This research was funded by the National Science Foundation through DMS-1715477, MRSEC DMR-1420570, ONR N00014-17-1-3029 and the Simons Foundation. SD acknowledges funding from the Smith Family Fellowship.

[1] T. Baumberger and C. Caroli, *Advances in Physics* **55**, 279 (2006).
 [2] Q. Li, T. E. Tullis, D. Goldsby, and R. W. Carpick, *letters to nature* **480**, 233 (2011).
 [3] L. Bocquet, E. Charlaix, S. Ciliberto, and J. Crassous, *letters to nature* **396**, 735 (1998).
 [4] M. Nakatani and H. Mochizuki, *Geophysical Research Letters* **23**, 869 (1996).
 [5] P. Berthoud, T. Baumberger, C. G’sell, and J. M.

Hiver, *Physical Review B* **59** (1999), 10.1103/PhysRevB.59.14313.
 [6] L. Bureau, T. Baumberger, and C. Caroli, *The European Physical Journal E* **8**, 331 (2002).
 [7] S. L. Karner and C. Marone, *Geophysical Monograph* (2000), 10.1029/GM120p0187.
 [8] S. L. Karner and C. Marone, *Geophysical Research Letters* **25**, 4561 (1998).
 [9] O. Ben-David and J. Fineberg, *Physical Review Letters* (2011), 10.1103/PhysRevLett.106.254301.
 [10] S. Dillavou and S. M. Rubinstein, *Physical Review Letters* **120**, 224101 (2018).
 [11] F. P. Bowden and D. Tabor, *The Friction and Lubrication of Solids* (Clarendon Press Oxford, 1950).
 [12] J. F. Archard, *Proceedings of the Royal Society A: Mathematical, Physical and Engineering Sciences*, 1 (1957).
 [13] J. A. Greenwood and J. B. P. Williamson, *Proceedings of the Royal Society A: Mathematical, Physical and Engineering Sciences* **295**, 300 (1966).
 [14] B. Persson, *The Journal of Chemical Physics* (2001), 10.1063/1.1388626.
 [15] J. H. Dieterich and B. D. Kilgore, *Pure and Applied Geophysics* **143**, 283 (1994).
 [16] B. Weber, T. Suhina, A. M. Brouwer, and D. Bonn, *Science Advances* **5**, eaav7603 (2019).
 [17] S. Dillavou and S. M. Rubinstein, *Physical Review Letters* **124**, 085502 (2020).
 [18] T. Pilvelait, S. Dillavou, and S. M. Rubinstein, *Physical Review Research* **2**, 012056 (2020).
 [19] S. M. Rubinstein, G. Cohen, and J. Fineberg, *letters to nature* (2004), 10.1038/nature02830.
 [20] I. Svetlizky and J. Fineberg, *letters to nature* **509**, 205 (2014).
 [21] J. H. Dieterich, *Journal of Geophysical Research* **84**, 2161 (1979).
 [22] J. R. Rice and A. Ruina, *Journal of Applied Mechanics* **50**, 343 (1983).
 [23] A. Ruina, *Journal of Geophysical Research* **88**, 10359 (1983).
 [24] P. Bhattacharya, A. M. Rubin, and N. M. Beeler, *Journal of Geophysical Research*, 1 (2017).
 [25] B. Rouet-Leduc, C. Hulbert, N. Lubbers, K. Barros, C. J. Humphreys, and P. A. Johnson, *Geophysical Research Letters* **44**, 9276 (2017).
 [26] C. Hulbert, B. Rouet-Leduc, P. A. Johnson, C. X. Ren, J. Rivière, D. C. Bolton, and C. Marone, *Nature Geoscience* **12**, 69 (2019).
 [27] T. Perol, M. Gharbi, and M. Denolle, *Science Advances* **4**, e1700578 (2018).
 [28] F. Corbi, L. Sandri, J. Bedford, F. Funicello, S. Brizzi, M. Rosenau, and S. Lallemand, *Geophysical Research Letters* **27**, 119 (2019).
 [29] J. McBeck, J. M. Aiken, Y. Ben-Zion, and F. Renard, *Earth and Planetary Science Letters* **543**, 116344 (2020).
 [30] E. D. Cubuk, S. S. Schoenholz, J. M. Rieser, B. D. Malone, J. Rottler, D. J. Durian, E. Kaxiras, and A. J. Liu, *Physical Review Letters* **114**, L08003 (2015).
 [31] Block Pair 1: $S = \{0, 5, 10, 15, 20, 25, 30, 35, 40\}$, $t = \{8, 32, 128, 512, 2048\}$. Block Pair 2: $S = \{0, 5, 10, 15, 20, 25, 30, 35, 40\}$, $t = \{16, 32, 64, 128, 256, 512\}$. Block Pair 3: $S = \{-30, -15, 0, 15, 30\}$, $t = \{8, 16, 64, 256, 1024\}$.
 [32] J. Hoffmann, Y. Bar-Sinai, L. M. Lee, J. Andrejevic, S. Mishra, S. M. Rubinstein, and C. H. Rycroft, *Sci-*

- ence Advances **5**, eaau6792 (2019).
- [33] K. P. Murphy, *Machine Learning: A Probabilistic Perspective* (MIT Press, Cambridge, MA, 2012).
- [34] For predicting data points that are the first (last) of a given S and t combination, the mean of the following (previous) two experiments are used.
- [35] S. Das and K. Aki, *Journal of Geophysical Research* **82**, 5658 (1977).